Customizing the mass and geometric stiffness of plane beam elements by Fourier methods

Carlos A. Felippa
Department of Aerospace Engineering Sciences and Center for Aerospace Structures, University of Colorado at Boulder, Boulder, Colorado, USA

Keywords *Finite element method, Beams, Vibration, Stiffness, Fourier's transform, Spectral analysis*

Abstract *Teaches by example the application of finite element templates in constructing high performance elements. The example discusses the improvement of the mass and geometric stiffness matrices of a Bernoulli-Euler plane beam. This process interweaves classical techniques (Fourier analysis and weighted orthogonal polynomials) with newer tools (finite element templates and computer algebra systems). Templates are parameterized algebraic forms that uniquely characterize an element population by a "genetic signature" defined by the set of free parameters. Specific elements are obtained by assigning numeric values to the parameters. This freedom of choice can be used to design "custom" elements. For this example weighted orthogonal polynomials are used to construct templates for the beam material stiffness, geometric stiffness and mass matrices. Fourier analysis carried out through symbolic computation searches for template signatures of mass and geometric stiffness that deliver matrices with desirable properties when used in conjunction with the well-known Hermitian beam material stiffness. For mass-stiffness combinations, three objectives are noted: high accuracy for vibration analysis, wide separation of acoustic and optical branches, and low sensitivity to mesh distortion and boundary conditions. Only the first objective is examined in detail.*

Introduction

A widely cited contribution of Ernest Hinton is his short article (Hinton *et al.*, 1976) on mass lumping schemes. Starting from a fully coupled mass matrix, which is usually the consistent mass matrix, the article recommends to lump by scaling the diagonal entries through an appropriate factor that preserves the total translational mass of the element. This procedure is now called the HRZ method. It is rated by Cook *et al.* (1989) as an effective lumping method for arbitrary elements. Although HRZ is not generally optimal for high order elements as shown by Malkus and Plesha (1986) and Malkus *et al.* (1988), it is straightforward to apply and leads to physically admissible behavior.

This contribution looks at mass matrices from a more general viewpoint. Specifically: which full or lumped mass matrices give good performance in

Preparation of the present paper has been supported by the National Science Foundation under Grant ECS-9725504, and by Sandia National Laboratories under the Advanced Strategic Computational Initiative (ASCI) Contract BF-3574.

Engineering Computations,
Vol. 18 No. 1/2, 2001, pp. 286-303.

dynamic analysis if only minimal constraints are placed on its entries? Is it the consistent mass? If not, how much can be gained from it? Can lumped mass matrices be competitive? A related problem arises in buckling and stability analysis: can one do better than merely using the consistent geometric stiffness?

Conventional error analysis in FEM cannot answer these questions. It only gives worst-case asymptotic convergence rates in some norm. This is like watchmaking with a sledgehammer. A sharper toolset is needed. Basic aspects of the methodology will be illustrated on a simple but non-trivial element: a plane Bernoulli-Euler beam. The exposition intends to show a balanced synthesis of the old and the new:

- weighted orthogonal bases;
- Fourier analysis;
- templates; and
- symbolic computations by computer algebra systems (CAS).

Orthogonal expansions and Fourier analysis are of course classical tools. Templates represent a frontier FEM subject still in the development stage. As regards the last tool, "Mathematica" was used to carry out the error-prone parametrized spectral computations required by templates, in minutes instead of days. So although CAS are not exactly new, their increasing power and availability on inexpensive desktops and laptops are gradually making possible the detailed analysis of 1D and 2D templates.

A plane beam is used because the element is well understood, fully displacement based, and exactly integrated. But it is not so trivial as, say, a two-node bar element. Hence the basic techniques can be explained in a short paper while giving some of the flavor of the far more complex algebraic manipulations that arise in plate and shell templates.

The beam element

The element under study is the two-node, prismatic, homogeneous, thin plane beam of length ℓ illustrated in Figure 1(a). The axes $\{x, y, z\}$ are placed

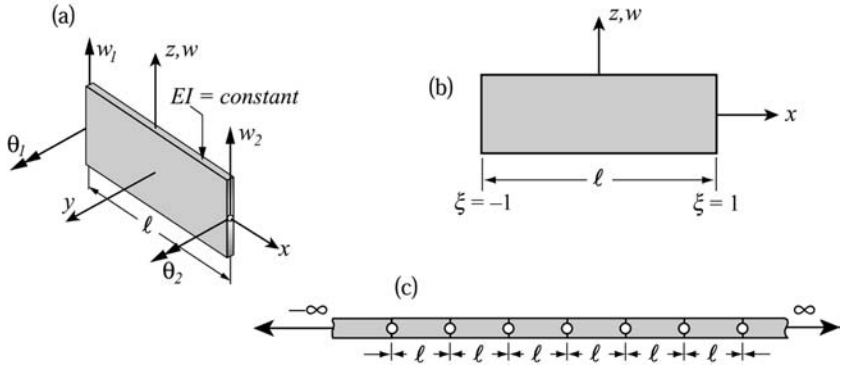

Figure 1.
(a) and (b) beam element under study. (c) Periodic lattice for Fourier analysis

as indicated. The isoparametric coordinate ξ is $-1 \leq \xi = 2x/\ell \leq 1$ as shown in Figure 1(b). Derivatives with respect to x and ξ will be abbreviated by prime and bullet supercripts, respectively: $(.)' \equiv d(.)/dx$ and $(.)^{\bullet} \equiv (2/\ell)(.)' = d(.)/d\xi$. The cross-section properties: area A and second moment of inertia $I \equiv I_{yy}$, as well as the material properties: elastic modulus E and density ρ, are assumed to be constant along x.

The kinematics of the Bernoulli-Euler beam model is fully determined by the transverse displacement field $w(x)$. The cross-section rotation is $\theta(x) = w'(x)$ and the curvature is $\kappa(x) = w''(x)$. In linear dynamics, the internal energy is:

$$\Pi = U_m - W = \frac{1}{2}\int_0^{\ell} EI\,\kappa^2\,dx - \int_0^{\ell} q\,w\,dx\,,$$

whereas the kinetic energy is:

$$T = \frac{1}{2}\int_0^{\ell} \rho A\,w^2\,dx\,.$$

For buckling analysis the energy functional is $\Pi = U_m + U_g$, with:

$$U_g = \frac{1}{2}\int_0^{\ell} P(w')^2\,dx\,,$$

in which P is the axial force.

The four degrees of freedom (DOFs) are the transverse end displacements $\{w_1, w_2\}$ and the length-scaled end rotations $\{r_1 = \ell\theta_1, r_2 = \ell\theta_2\}$. Use of $\{r_1, r_2\}$ renders all equations dimensionally homogeneous. Although in actual FEM analysis the rotational freedoms are $\{\theta_1, \theta_2\}$, ℓ-scaling is possible here because Fourier analysis is carried out on the infinite periodic-lattice structure depicted in Figure 1(c).

Displacement bases

The two cubic-displacement bases depicted in Figures 2 and 3 will be considered in this study.

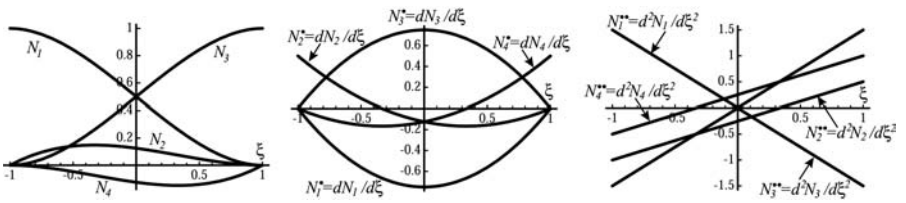

Figure 2.
The Hermite interpolation functions and their derivatives

Hermite interpolation shape functions

These are the well known Hermite cubic interpolation functions, also called shape functions, which may be found in any FEM textbook (e.g. Cook *et al.*, 1989). (They should not be confused with "Hermite polynomials", which are a totally different thing.) Along with their first and second x derivatives they are collected in the row vectors:

$$\begin{aligned}\mathbf{N} &= [N_1 \quad N_2 \quad N_3 \quad N_4\,], \quad \mathbf{N}' = [N_1' \quad N_2' \quad N_3' \quad N_4'\,], \\ \mathbf{N}'' &= [N_1'' \quad N_2'' \quad N_3'' \quad N_4''\,],\end{aligned} \tag{1}$$

in which:

$$\begin{aligned}&N_1 = \frac{1}{4}(1-\xi)^2(2+\xi), \;\; N_2 = \frac{1}{8}(1-\xi)^2(1+\xi), \;\; N_3 = \frac{1}{4}(1+\xi)^2(2-\xi), \\ &N_4 = -\frac{1}{8}(1+\xi)^2(1-\xi).\end{aligned} \tag{2}$$

These functions are depicted in Figure 2 along with first and second ξ derivatives. They interpolate directly w from the end freedoms: $w = w_1N_1 + r_1N_2 + w_2N_3 + r_2N_4$. Product integration over the length provides the Hermitian covariance matrices for prismatic beams:

$$\mathbf{Q}_H = \int_{-\ell/2}^{\ell/2} \mathbf{N}\,\mathbf{N}^T\,dx = \frac{\ell}{420}\begin{bmatrix} 156 & 22 & 54 & -13 \\ 22 & 4 & 13 & -3 \\ 54 & 13 & 156 & -22 \\ -13 & -3 & -22 & 4 \end{bmatrix}, \tag{3}$$

$$\mathbf{R}_H = \int_{-\ell/2}^{\ell/2} \mathbf{N}'\,(\mathbf{N}')^T\,dx = \frac{1}{30\ell}\begin{bmatrix} 36 & 3 & -36 & 3 \\ 3 & 4 & -3 & -1 \\ -36 & -3 & 36 & -3 \\ 3 & -1 & -3 & 4 \end{bmatrix}, \tag{4}$$

$$\mathbf{S}_H = \int_{-\ell/2}^{\ell/2} \mathbf{N}''\,(\mathbf{N}'')^T\,dx = \frac{1}{\ell^3}\begin{bmatrix} 12 & 6 & -12 & 6 \\ 6 & 4 & -6 & 2 \\ -12 & -6 & 12 & -6 \\ 6 & 2 & -6 & 4 \end{bmatrix}. \tag{5}$$

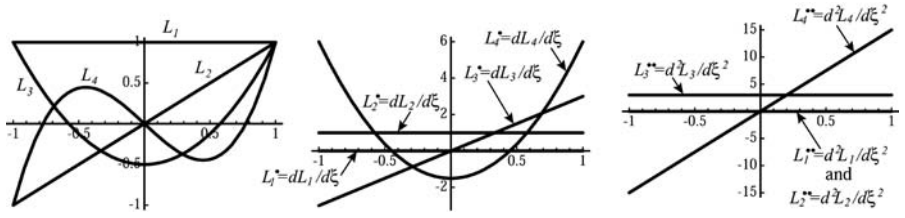

Figure 3.
The Legendre polynomial functions and their derivatives

Using the scaling matrix $\mathbf{W} = \mathbf{diag}[1, \ell, 1, \ell]$, the Hermitian material stiffness matrix, consistent geometric stiffness matrix and consistent mass matrix of the beam element are $\mathbf{K}_m = EI\,\mathbf{W}^T\mathbf{S}_H\,\mathbf{W}$, $\mathbf{K}_g = P\,\mathbf{W}^T\mathbf{R}_H\mathbf{W}$ and $\mathbf{M} = \rho A\,\mathbf{W}^T\mathbf{Q}_H\,\mathbf{W}$, respectively.

Legendre polynomials

The second basis considered here is also well known. It is formed by the first four Legendre polynomials:

$$\begin{aligned}\mathbf{L} &= [L_1 \quad L_2 \quad L_3 \quad L_4], \quad \mathbf{L}' = [L_1' \quad L_2' \quad L_3' \quad L_4'],\\ \mathbf{L}'' &= [L_1'' \quad L_2'' \quad L_3'' \quad L_4''],\end{aligned} \tag{6}$$

with:

$$L_1(\xi) = 1, \quad L_2(\xi) = \xi, \quad L_3(\xi) = \tfrac{1}{2}(3\xi^2 - 1), \quad L_4(\xi) = \tfrac{1}{2}(5\xi^3 - 3\xi). \tag{7}$$

This is a FEM oriented nomenclature; L_1 through L_4 are called P_0 through P_3 in mathematical handbooks; for example Chapter 22 of Abramowitz and Stegun (1964). They are normalized as per the usual conventions: $L_i(1) = 1$, $L_i(-1) = (-1)^{i-1}$. These polynomials and their first two derivatives are plotted in Figure 3. The resultant displacement interpolation is:

$$w = L_1\,q_1 + L_2\,q_2 + L_3\,q_3 + L_4\,q_4 = \mathbf{L}\,\mathbf{q}. \tag{8}$$

The amplitudes q_i are generalized coordinates, which are related to the element DOFs by the transformations:

$$\begin{aligned}\begin{bmatrix} w_1 \\ r_1 \\ w_2 \\ r_2 \end{bmatrix} &= \begin{bmatrix} 1 & -1 & 1 & -1 \\ 0 & 2 & -6 & 12 \\ 1 & 1 & 1 & 1 \\ 0 & 2 & 6 & 12 \end{bmatrix} \begin{bmatrix} q_1 \\ q_2 \\ q_3 \\ q_4 \end{bmatrix} = \mathbf{G}\mathbf{q},\\ \begin{bmatrix} q_1 \\ q_2 \\ q_3 \\ q_4 \end{bmatrix} &= \frac{1}{60} \begin{bmatrix} 30 & 5 & 30 & -5 \\ -36 & -3 & 36 & -3 \\ 0 & -5 & 0 & -5 \\ 6 & 3 & -6 & 3 \end{bmatrix} \begin{bmatrix} w_1 \\ r_1 \\ w_2 \\ r_2 \end{bmatrix} = \mathbf{H}\mathbf{u}.\end{aligned} \tag{9}$$

Here $\mathbf{G} = \mathbf{H}^{-1}$. This follows the standard notation of the free formulation as presented by Bergan and Nygård (1984) and Bergan and Felippa (1985). The function inner-product integrals over the element length give the covariance matrices:

$$\mathbf{Q} = \int_{-\ell/2}^{\ell/2} \mathbf{L}\,\mathbf{L}^T\,dx = \ell \begin{bmatrix} 1 & 0 & 0 & 0 \\ 0 & 1/3 & 0 & 0 \\ 0 & 0 & 1/5 & 0 \\ 0 & 0 & 0 & 1/7 \end{bmatrix}, \tag{10}$$

$$\mathbf{R} = \int_{-\ell/2}^{\ell/2} \mathbf{L}'(\mathbf{L}')^T \, dx = \frac{4}{\ell} \begin{bmatrix} 0 & 0 & 0 & 0 \\ 0 & 1 & 0 & 1 \\ 0 & 0 & 3 & 0 \\ 0 & 1 & 0 & 6 \end{bmatrix}, \tag{11}$$

$$\mathbf{S} = \int_{-\ell/2}^{\ell/2} \mathbf{L}'' \, (\mathbf{L}'')^T \, dx = \frac{48}{\ell^3} \begin{bmatrix} 0 & 0 & 0 & 0 \\ 0 & 0 & 0 & 0 \\ 0 & 0 & 3 & 0 \\ 0 & 0 & 0 & 25 \end{bmatrix}. \tag{12}$$

As can be observed L_i and their second derivatives are orthogonal over the beam length, whereas their first derivatives are not.

This representation is more useful than the Hermite basis for developing templates for beam elements, because the Legendre functions are "hierarchical" in nature and have clear physical meaning. Polynomials L_1 and L_2 represent translational and rotational rigid motions, respectively, L_3 is a constant-curvature symmetric bending mode and, finally, L_4 is a linear-curvature antisymmetric bending mode. For Timoshenko beam models, L_4 is a constant shear mode.

Templates

A finite element template, or simply "template", is an algebraic form that represents element-level equations, and which fulfills the following conditions:

- consistency (C);
- stability (correct rank) (S);
- observer invariance (I); and
- parametrization (P).

These are discussed at length in other papers, for example Felippa *et al.* (1995) and Felippa (2000). The first two conditions, (C) and (S), are imposed to ensure convergence as the mesh size is reduced by enforcing a priori satisfaction of the individual element test of Bergan and Hanssen (1975). Condition (P) means that the template contains free parameters; this permits performance optimization as well as tuning elements, or combinations of elements, to fulfill specific needs. Setting the free parameters to numeric values yields specific element instances. The set of free parameters is called the template "signature", a term introduced in Felippa and Militello (1999) and Felippa (1999). Borrowing terminology from biogenetics, the signature may be viewed as an "element DNA" that uniquely characterizes the instance. Elements derived by different techniques that share the same signature are called "clones".

Full mass and material stiffness templates

Templates for the full mass and material stiffness are easily obtained by scaling the entries of the covariance matrices **Q** and **S** as follows:

$$\mathbf{Q}^{\mu} = \mathbf{Q}(\mu_1, \mu_2, \mu_3) = \ell \begin{bmatrix} 1 & 0 & 0 & 0 \\ 0 & \mu_1/3 & 0 & 0 \\ 0 & 0 & \mu_2/5 & 0 \\ 0 & 0 & 0 & \mu_3/7 \end{bmatrix},$$
$$\mathbf{S}^{\beta} = \mathbf{S}(\beta) = \frac{48}{\ell^3} \begin{bmatrix} 0 & 0 & 0 & 0 \\ 0 & 0 & 0 & 0 \\ 0 & 0 & 3 & 0 \\ 0 & 0 & 0 & 25\beta \end{bmatrix}, \tag{13}$$

under the constraints $\mu_i \geq 0$, $i = 1, 2, 3$ and $\beta > 0$. This generalization can be obtained by reinterpreting the integrals (12) and (10) in a Riemann-Stieltjes or "distribution" sense. In practice it is not necessary to think of esoteric mathematics. The recipe is: traverse down the main diagonal of the covariance matrix, and scale the diagonal coefficients that follow the first non-zero entry.

Notice that the first non-zero diagonal entry must not be parametrized. This is a consequence of the template consistency or (C) requirement, which can be viewed as a conservation condition. The physical interpretation is: the element rigid-translational mass must be preserved, and the stiffness response to a constant curvature state must be exact. The stability or (S) condition restricts the three mass parameters to be non-negative and the stiffness parameter to be positive non-zero.

The parametrized full-mass and material stiffness matrices are:

$$\widehat{\mathbf{M}}^{\mu} = \rho A\, \mathbf{H}^T \mathbf{Q}^{\mu}_{\ell}\, \mathbf{H}, \quad \widehat{\mathbf{K}}^{\beta}_{m} = EI\, \mathbf{H}^T \mathbf{S}^{\beta}_{\ell}\, \mathbf{H}, \tag{14}$$

where $\widehat{(.)}$ distinguishes matrices in terms of the homogenized freedoms $\{w_1, r_1, w_2, r_2\}$. These have the following spectral representations as sum of rank-one matrices:

$$\begin{aligned} \hat{\mathbf{M}}^{\mu} = \rho A \ell \Bigg(& \frac{1}{144} \begin{bmatrix} 36 & 6 & 36 & -6 \\ 6 & 1 & 6 & -1 \\ 36 & 6 & 36 & -6 \\ -6 & -1 & -6 & 1 \end{bmatrix} \\ & + \frac{\mu_1}{1{,}200} \begin{bmatrix} 144 & 12 & -144 & 12 \\ 12 & 1 & -12 & 1 \\ -144 & -12 & 144 & -12 \\ 12 & 1 & -12 & 1 \end{bmatrix} \\ & + \frac{\mu_2}{720} \begin{bmatrix} 0 & 0 & 0 & 0 \\ 0 & 1 & 0 & -1 \\ 0 & 0 & 0 & 0 \\ 0 & -1 & 0 & 1 \end{bmatrix} + \frac{\mu_3}{2{,}800} \begin{bmatrix} 4 & 2 & 4 & 2 \\ 2 & 1 & -2 & 1 \\ 4 & -2 & 4 & -2 \\ 2 & 1 & -2 & 1 \end{bmatrix} \Bigg), \end{aligned} \tag{15}$$

$$\hat{\mathbf{K}}_m^{\beta} = \frac{EI}{\ell^3}\left(\begin{bmatrix} 0 & 0 & 0 & 0 \\ 0 & 1 & 0 & -1 \\ 0 & 0 & 0 & 0 \\ 0 & -1 & 0 & 1 \end{bmatrix} + \beta \begin{bmatrix} 12 & 6 & -12 & 6 \\ 6 & 3 & -6 & 3 \\ -12 & -6 & 12 & -6 \\ 6 & 3 & -6 & 3 \end{bmatrix} \right). \tag{16}$$

Setting $\mu_1 = \mu_2 = \mu_3 = \beta = 1$ produces the well known consistent mass and material stiffness matrix, respectively, associated with the Hermitian basis.

Lumped mass template

To include block-diagonal-lumped mass matrices in this study we introduce directly the two-parameter template:

$$\widehat{\mathbf{M}}_L^{\nu} = \widehat{\mathbf{M}}(\nu_1, \nu_2) = \rho A\, \ell \begin{bmatrix} \frac{1}{2} & \nu_2 & 0 & 0 \\ \nu_2 & \nu_1 & 0 & 0 \\ 0 & 0 & \frac{1}{2} & -\nu_2 \\ 0 & 0 & -\nu_2 & \nu_1 \end{bmatrix}, \tag{17}$$

where $\nu_1 \geq 0$ and $\nu_1 \geq \nu_2^2$ to maintain non-negativity. Diagonal lumped matrices are obtained if $\nu_2 = 0$. The only common instance of $\widehat{\mathbf{M}}(\mu_1, \mu_2, \mu_3)$ and $\widehat{\mathbf{M}}_L(\nu_1, \nu_2)$ is $\widehat{\mathbf{M}}(5/3, 5, 35) \equiv \widehat{\mathbf{M}}_L(1/36, 1/12)$.

Geometric stiffness template

The covariance matrix $\mathbf{R}$, given by equation (11), which appears in the geometric stiffness is non-diagonal because of the coupling of L_2' and L_4'. To produce a diagonal covariance the last polynomial is changed to $\tilde{L}_4(\xi) = L_4 - L_2 = 5\xi(1-\xi^2)/2$. This is not a Legendre polynomial because it vanishes at $\xi = \pm 1$, but its derivative is. The new covariance matrix is $\tilde{\mathbf{R}} = (4/\ell)\,\mathbf{diag}[\,0 \quad 1 \quad 3 \quad 5\,]$, which parametrizes to:

$$\tilde{\mathbf{R}}^{\gamma} = \tilde{\mathbf{R}}(\gamma_1, \gamma_2) = \frac{4}{\ell} \begin{bmatrix} 0 & 0 & 0 & 0 \\ 0 & 1 & 0 & 0 \\ 0 & 0 & 3\gamma_1 & 0 \\ 0 & 0 & 0 & 5\gamma_2 \end{bmatrix}, \tag{18}$$

in which $\gamma_1 \geq 0$ and $\gamma_2 \geq 0$. Using $w = L_1\,\tilde{q}_1 + L_2\,\tilde{q}_2 + L_3\,\tilde{q}_3 + \tilde{L}_4\,\tilde{q}_4$ the freedom transformation matrices are reworked:

$$\begin{bmatrix} w_1 \\ r_1 \\ w_2 \\ r_2 \end{bmatrix} = \begin{bmatrix} 1 & -1 & 1 & 0 \\ 0 & 2 & -6 & -10 \\ 1 & 1 & 1 & 0 \\ 0 & 2 & 6 & -10 \end{bmatrix} \begin{bmatrix} \tilde{q}_1 \\ \tilde{q}_2 \\ \tilde{q}_3 \\ \tilde{q}_4 \end{bmatrix} = \tilde{\mathbf{G}}\mathbf{q}, \qquad \begin{bmatrix} \tilde{q}_1 \\ \tilde{q}_2 \\ \tilde{q}_3 \\ \tilde{q}_4 \end{bmatrix} = \frac{1}{60} \begin{bmatrix} 30 & 5 & 30 & -5 \\ -30 & 0 & 30 & 0 \\ 0 & -5 & 0 & -5 \\ -6 & -3 & 6 & -3 \end{bmatrix} \begin{bmatrix} w_1 \\ r_1 \\ w_2 \\ r_2 \end{bmatrix} = \tilde{\mathbf{H}}\mathbf{u}. \tag{19}$$

The spectral form of the geometric stiffness template $\widehat{\mathbf{K}}_g^{\gamma} = P\,\tilde{\mathbf{H}}^T\tilde{\mathbf{R}}^{\gamma}\tilde{\mathbf{H}}$ is:

$$\widehat{\mathbf{K}}_g^{\gamma} = \frac{P}{\ell}\left(\begin{bmatrix} 1 & 0 & -1 & 0 \\ 0 & 0 & 0 & 0 \\ -1 & 0 & 1 & 0 \\ 0 & 0 & 0 & 0 \end{bmatrix} + \frac{\gamma_1}{12} \begin{bmatrix} 0 & 0 & 0 & 0 \\ 0 & 1 & 0 & -1 \\ 0 & 0 & 0 & 0 \\ 0 & -1 & 0 & 1 \end{bmatrix} + \frac{\gamma_2}{60} \begin{bmatrix} 12 & 6 & -12 & 6 \\ 6 & 3 & -6 & 3 \\ -12 & -6 & 12 & -6 \\ 6 & 3 & -6 & 3 \end{bmatrix} \right). \tag{20}$$

This hierarchical form has an interesting historical interpretation. The first term is the rank-one geometric stiffness of the two-node bar element, which was used for framework buckling analysis in the early 1960; see for example Argyris *et al.* (1964). Later Martin (1966) formulated the consistent geometric stiffness, which may be obtained by setting $\gamma_1 = \gamma_2 = 1$ in equation (20), and reported a significant increase in accuracy for the same FEM discretization. An intermediate rank-two form, not available in the literature, is obtained by setting $\gamma_1 = 1$ and $\gamma_2 = 0$. This illustrates the power of templates to subsume all possible elements in one expression.

Mass-stiffness Fourier analysis

To assess the performance of mass-stiffness combinations for dynamics we perform Fourier analysis of the infinite beam lattice of Figure 1(c), taking the typical three-node $\{i, j, k\}$ patch shown in Figure 4. The operational techniques introduced by Park and Flaggs (1984a; 1984b) for element analysis are followed. The unforced semidiscrete dynamical equations of the patch are:

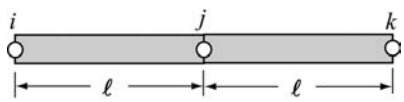

Figure 4.
Three-node repeating patch for Fourier analysis

$$\mathbf{M}_P^{\mu}\,\ddot{\mathbf{u}}_P + \mathbf{K}_P^{\beta}\,\mathbf{u}_P = \mathbf{0}, \tag{21}$$

in which a superposed dot denotes differentiation with respect to time t, and:

$$\begin{aligned}
\mathbf{u}_P &= [\,w_i \quad r_i \quad w_j \quad r_j \quad w_k \quad r_k\,]^T \\
\mathbf{M}_P^{\mu} &= \rho A\,\ell \begin{bmatrix} 36(175-84\mu_1-\mu_3) & 6(175-42\mu_1-3\mu_3) \\ -6(175-42\mu_1-3\mu_3) & 175+21\mu_1-35\mu_2+9\mu_3 \\ 72(175+84\mu_1+\mu_3) & 0 \\ 0 & 2(175+21\mu_1+35\mu_2+9\mu_3) \\ 36(175-84\mu_1-\mu_3) & -6(175-42\mu_1-3\mu_3) \\ 6(175-42\mu_1-3\mu_3) & -175+21\mu_1-35\mu_2+9\mu_3 \end{bmatrix} \\
\mathbf{K}_P^{\beta} &= \frac{EI}{\ell^3} \begin{bmatrix} -12\beta & -6\beta & 24\beta & 0 & -12\beta & 6\beta \\ 6\beta & -1+3\beta & 0 & 2+6\beta & -6\beta & -1+3\beta \end{bmatrix}
\end{aligned} \tag{22}$$

Plane wave propagation

We study the propagation over the lattice of plane waves of wavelength L, wavenumber $k_p = 2\pi/L$, and circular frequency ω_p:

$$w(x,t) = A\,e^{i(k_p x-\omega_p t)}, \quad r(x,t) = \ell\,\theta(x,t) = B\,e^{i(k_p x-\omega_p t)}, \tag{23}$$

in which subscript p means "physical". To simplify the subsequent analysis we will work with the dimensionless frequency $\omega^2 = \omega_p^2/(EI/\rho A\ell^3)$ and wavenumber $k = k_p\ell$. The dimensionless wavespeed is $c = \omega/k$. A curve plotting solution $\omega = \omega(k)$ of equation (23) is called a "dispersion relation".

Evaluating equation (23) at the nodes $\{i,j,k\}$, inserting into equation (21), dropping the time dependency and requiring plane wave solutions with non-zero A,B yields a frequency equation biquadratic in ω that has non-negative real roots. For convenience define $\psi_1 = 60 + 5\mu_1 + \mu_2$, $\psi_2 = 15\mu_1 - \mu_2 - 20$, $\psi_3 = 28\mu_2 - 5\mu_3 + 35$, $\psi_4 = \mu_2 + 20$, $\psi_5 = \mu_2 - 40$, $\psi_6 = 36\mu_2 + 285$, $\psi_7 = 84\mu_1 + \mu_3$, $\psi_8 = 4\mu_2 + 15$, $\psi_9 = 36\mu_1 + 5\beta\psi_1 + 25$, $\psi_{10} = 5\beta\psi_2 - 36\mu_1 + 75$, $\psi_{11} = 140\beta\psi_5 + 12\psi_7$, $\psi_{12} = 7\psi_{10} - 3\mu_3$, $\psi_{13} = -21\psi_9 - 9\mu_3$, $\psi_{14} = 84\mu_1\psi_8 + 4\psi_5\mu_3$, $\psi_{15} = 3\mu_1\psi_3 - 175\mu_2 + \psi_4\mu_3$, $\psi_{16} = 175\mu_2 + 7\mu_1\psi_6 + 3\psi_1\mu_3$, $\phi_1 = -\psi_{13} - \psi_{11}\cos k - \psi_{12}\cos 2k$ and $\phi_2 = \psi_{16} - \psi_{14}\cos k + \psi_{15}\cos 2k$. Then the frequency-wavenumber relation obtained by "Mathematica" can be succintly written as:

$$\begin{matrix} \omega_a^2 \\ \omega_o^2 \end{matrix} = \frac{120}{\phi_2}\left(\phi_1 \mp \sqrt{\phi_1^2 - 3{,}360\,\beta\phi_2\,\sin^4\tfrac{1}{2}k}\right). \tag{24}$$

Frequencies ω_a^2 and ω_o^2, which depend on the four free parameters $\{\beta,\mu_1,\mu_2,\mu_3\}$, pertain to the so-called acoustic and optical branches, respectively; a nomenclature explained by Brillouin (1946). Only the acoustic branch appears in the continuum BE model, for which $\omega^2 = k^4$ (see, for example, Graff, 1991). The

optical branch is introduced by the FEM discretization and corresponds to high-frequency lattice oscillations or "mesh modes", as discussed by Belytschko and Mullen (1978). The Taylor expansion about $k = 0$, which is of interest in low-frequency accuracy studies, contains only even powers of k:

$$\begin{aligned}\omega_a^2 &= k^4 - \frac{1+\beta(\mu_1-2)}{12\beta}k^6 \\ &\quad + \frac{5+\beta\big(3\mu_1+\beta(9+5\mu_1^2-10\mu_1-\mu_2)-10\big)}{720\beta^2}k^8 + O(k^{10}), \\ \omega_o^2 &= \frac{25{,}200\beta}{7\mu_1+3\mu_3} + \frac{2{,}100\big(7(\mu_1-10\beta\mu_1+\beta\mu_1^2-5\beta\mu_2)+3\mu_3\big)}{(7\mu_1+3\mu_3)^2}k^2 \\ &\quad + O(k^4).\end{aligned} \tag{25}$$

Only a few leading terms are shown since succeeding ones, found by "Mathematica" through $O(k^{14})$, get increasingly complicated. If one selects:

$$\mu_1 = \frac{2\beta-1}{\beta}, \qquad \mu_2 = \frac{7-14\beta+9\beta^2}{\beta^2}, \qquad \mu_3 = \frac{245-546\beta+427\beta^2-100\beta^3}{3\beta}. \tag{26}$$

then the coefficients of k^6, k^8 and k^{10} in the first part of equation (25) vanish, and $\omega_a^2 = k^4 + O(k^{12})$. The coefficient of k^{12}, which is $-(125\beta^4 - 182\beta^3 - 147\beta^2 + 196\beta + 49)/(18{,}144{,}000\beta^4)$ cannot be zeroed out for any positive real value of β, but is very approximately minimized by taking $\beta = 4/3$.

A similar analysis with the lumped mass template (17) leads to a dispersion relation that depends on two parameters: $\{\beta, \nu_1\}$ because the effect of ν_2 cancels out on a regular lattice:

$$\frac{\omega_a^2}{\omega_o^2} = \frac{1+\beta\chi_1+(\beta\chi_2-1)\cos k \mp \sqrt{\big[1+\beta\chi_1+(\beta\chi_2-1)\cos k\big]^2 - 384\beta\nu_1\sin^4 k}}{2\nu_1}, \tag{27}$$

in which $\chi_1 = 3 + 24\nu_1$ and $\chi_2 = 3 - 24\nu_1$. The Taylor expansions about $k = 0$ are:

$$\begin{aligned}\omega_a^2 &= k^4 + \frac{\beta-1-24\beta\nu_1}{12\beta}k^6 \\ &\quad + \frac{5+3\beta\big(120\nu_1-5+3\beta\big(1-40\nu_1+320\nu_1^2\big)\big)}{720\beta^2}k^8 + O(k^{10}), \\ \omega_o^2 &= \frac{6\beta}{\nu_1} + \frac{1-3\beta+24\beta\nu_1}{2\nu_1}k^2 + O(k^4).\end{aligned} \tag{28}$$

If $\nu_1 = \frac{1}{24}(\beta - 1)/\beta$ the coefficient of k^6 vanishes. If $\beta = (5 - \sqrt{5})/2$ and $\nu_1 = (5 - \sqrt{5})/240$ the coefficients of k^6 and k^8 vanish.

Figures 5 and 6 plot the acoustic and optical branches showing $|\omega_a|$ and $|\omega_o|$, respectively, as functions of k, for the eight mass-stiffness combinations listed in Table I. These combinations possess either historical or practical interest. (The significance of the acronyms is discussed below.) Branches are shown for $k \in [0, 2\pi]$ and repeat with period 2π. The interval $-\pi \leq k \leq \pi$ is called the "first Brillouin zone". The vertical distance between the maximum of ω_a, which often happens at $k = \pi$, and the maximum of ω_a, is called the "stopping band" or "forbidden band", a term derived from filter technology.

Multiobjective parameter selection

The four parameters of the full-mass plus stiffness template or the three parameters of the lumped-mass plus stiffness template may be used to achieve various performance goals. Three important ones are:

(1) *Objective A*. Low frequency accuracy in the sense that ω_a^2 agrees well with k^4 as $k \to 0$. This is of interest for structural dynamics, in which low frequency behavior dominates.

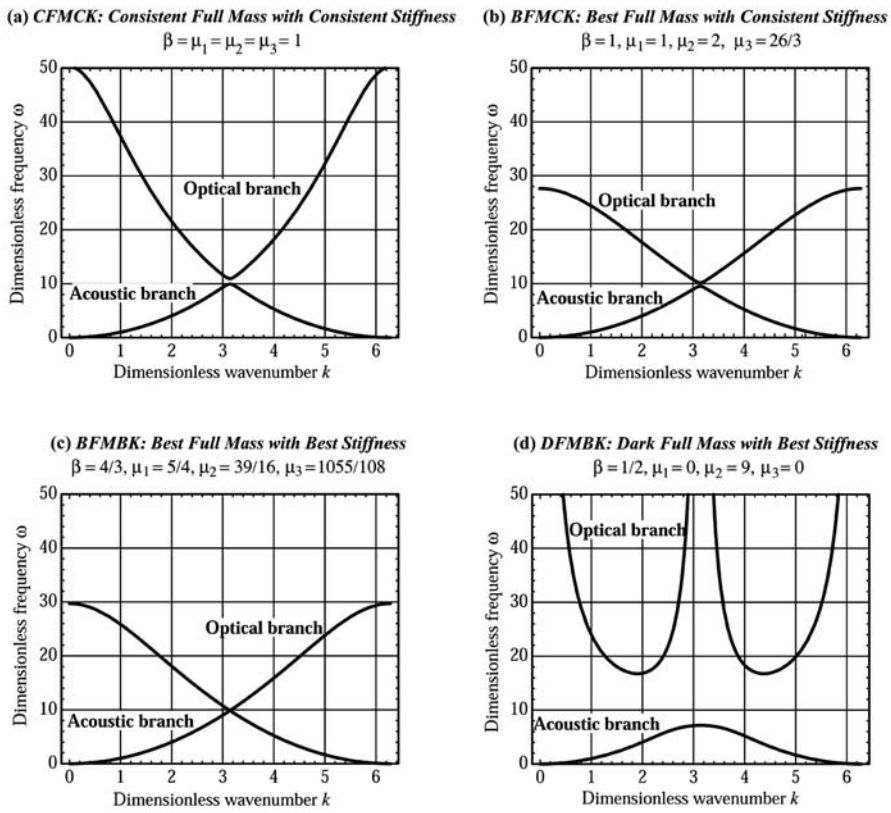

Figure 5.
Dispersion relation for four full-mass-matrix template instances

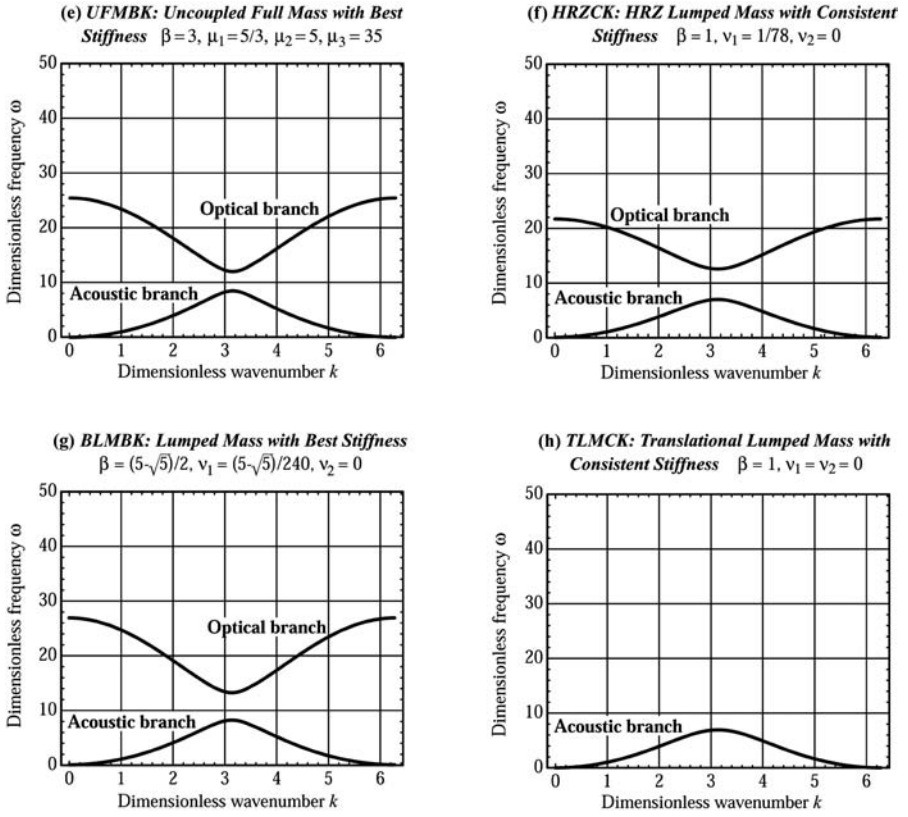

Figure 6.
Dispersion relations for four lumped-mass-matrix template instances

Acronym	Template signature β	μ_1	μ_2	μ_3	ν_1	ν_2	Low frequency ($k \to 0$) Taylor expansion of ω_a^2	Distortion sensitivity
CFMCK	1	1	1	1			$k^4 + \frac{k^8}{720} - \frac{k^{10}}{25{,}200} + \frac{k^{12}}{604{,}800} + O(k^{14})$	Low
BFMCK	1	1	2	$\frac{26}{3}$			$k^4 - \frac{41\,k^{12}}{18{,}144{,}000} + O(k^{14})$	Medium
BFMBK	$\frac{4}{3}$	$\frac{5}{4}$	$\frac{39}{16}$	$\frac{1{,}055}{108}$			$k^4 - \frac{41\,k^{12}}{185{,}794{,}560} + O(k^{14})$	Very high
DFMBK	$\frac{1}{2}$	0	9	0			$k^4 + \frac{53\,k^{10}}{30{,}240} - \frac{13\,k^{12}}{34{,}560} + O(k^{14})$	High
UFMBK	3	$\frac{5}{3}$	5	35			$k^4 + \frac{k^8}{6{,}480} - \frac{k^{10}}{13{,}608} - \frac{107\,k^{12}}{20{,}995{,}200} + O(k^{14})$	Medium
UFMBK	3				$\frac{1}{36}$	$\frac{1}{12}$	Same as above – UFMBK has two signatures	
HRZCK	1				$\frac{1}{78}$	0	$k^4 - \frac{k^6}{39} - \frac{89\,k^8}{121{,}680} - \frac{151\,k^8}{1{,}845{,}480} + \frac{239{,}329\,k^{12}}{51{,}821{,}078{,}400} + O(k^{14})$	Low
BLMBK	$\frac{5-\sqrt{5}}{2}$				$\frac{5-\sqrt{5}}{240}$	0	$k^4 - \frac{k^{10}}{10{,}080} - \frac{k^{12}}{129{,}600} + O(k^{14})$	High
TLMCK	1				0	0	$k^4 - \frac{k^8}{720} - \frac{k^{10}}{3{,}024} - \frac{7\,k^{12}}{259{,}200} + O(k^{14})$	Low

Table I.
Eight interesting mass stiffness combinations

(2) *Objective B*. Wide forbidden band between acoustic and optical branches. This is of interest in wave propagation dynamics to reduce spurious noise, particularly at discontinuous wavefronts.

(3) *Objective S*. Low sensitivity of frequency predictions to mesh distortion and boundary conditions. This goal is self-explanatory: it tries to lessen effects of the deviation from the infinite regular lattice assumed in classical Fourier analysis.

Ideally, the parameters should be chosen to improve performance in the three objectives. Unfortunately they are not compatible, and they should be weighted depending on the intended application. For all-around use in general purpose codes, a compromise may be necessary.

Existing mass-stiffness combinations

Before discussing parameter selection it is of interest to note how existing elements fare in objectives A and B. Table I lists three well-known combinations: CFMCK, TLMCK and HRZCK. The combination of consistent full mass and consistent stiffness, called CFMCK is obtained if $\beta = \mu_1 = \mu_2 = \mu_3 = 1$. The simplest lumped mass matrix corresponds to $\nu_1 = \nu_2 = 0$, which has only translational point masses and zero rotational masses; when used in conjunction with the consistent stiffness $\beta = 1$, this combination is called TLMCK. The HRZ lumped mass matrix described in the Introduction, is defined by $\nu_1 = 1/78$ and $\nu_2 = 0$ and is used together with the consistent stiffness $\beta = 1$ in HRZCK. The Taylor expansions of ω_a^2 given in Table I show that CFMCK and TLMCK achieve low frequency accuracy of $O(h^4)$, $h = \ell/L$, in $|\omega_a|$. The sign of the first truncation term indicates that CFMCK overestimates $|\omega_a|$ whereas TLMCK underestimates it, which is a well-known property. Using the average mass would give higher accuracy. Although HRZCK has low accuracy order it will be later seen to be distortion insensitive.

New mass-stiffness combinations

Achieving objective A (high low-frequency accuracy) is easy if one forgets about the other two. Using the selection rule (equation (26)) with $\beta = 1$ and $\beta = 4/3$ provides combinations called BFMCK (best full mass and consistent stiffness) and BFMBK (best full mass and best stiffness), respectively. These possess accuracy of $O(h^4)$ for $|\omega_a|$ on an infinite regular lattice. BFMBK displays very nearly the lowest truncation error in ω_a^2 and practically represents the most that can be "squeezed out" of the full-mass-stiffness template if objectives B and S are ignored. Combination BLMBK (best lumped mass and best stiffness) is obtained with $\beta = (5 - \sqrt{5})/2 \approx 1.382$ and $\nu_1 = (5 - \sqrt{5})/240 \approx 1/87$, which gives the most accurate lumped-mass-stiffness template.

Combination DFMBK ((optically) dark full mass with best stiffness) attempts to fulfill both objectives A and B by moving the optical branch upward while maintaining reasonable accuracy in low frequencies. This is

done by enforcing $\omega_o^2 \to \infty$ as $k \to 0$. A glance at the second part of equation (25) shows that this requires $7\mu_1 + 3\mu_3 = 0$, but since both parameters must be non-negative the only possibility is $\mu_1 = \mu_3 = 0$. Taking $\beta = 3$ and $\mu_2 = 9$ makes the coefficients of k^6 and k^8 in ω_a^2 vanish, although the coefficient of k^{10} remains quite large compared to other elements. This mass matrix has one blemish: it is rank deficient.

The combination UFMBK (uncoupled full mass with best stiffness) adopts $\mu_1 = 5/3$, $\mu_2 = 5$ and $\mu_3 = 35$, a signature that makes $\mathbf{M}^\mu$ block diagonal. Taking $\beta = 1/2$ makes the coefficient of k^6 vanish. This instance is exhibited as a curiosity since its mass is the only one that is a member of both the full-mass and lumped-mass templates. For the latter it can be obtained by setting $\nu_1 = 1/36$ and $\nu_2 = 1/12$.

Vibration analysis example

The performance of the eight combinations of Table I in vibration analysis of a simply-supported (SS) prismatic beam of length L divided into N equal elements is shown in Figure 7. This is a log-log plot that displays the error in the first two dimensionless fundamental frequencies $|\omega_1| = \pi^2$ and $|\omega_2| = 4\pi^2$ as functions of N = 1, 2, . . . 32. (The physical frequencies are $\omega_{1p} = \pi^2\sqrt{EI/(\rho AL^3)}$ and $\omega_{2p} = 4\pi^2\sqrt{EI/(\rho AL^3)}$.) The error is plotted as $d = \log_{10}(|\omega_{computed} - \omega_{exact}|)$, which gives at a glance the number of correct digits.

The computed results correlate well with the truncation analysis of ω_a^2 in Table I. This can be expected not only because the mesh is uniform, but (most importantly) the eigenfunctions of a SS beam are sinusoidal, which agrees with the plane wave spatial distribution (equation (23)). The high accuracy of BFMCK and BFMBK should be noted. For example, four BFMBK elements give $|\omega_1|$ to seven figures: 9.86960424 . . . versus $\pi^2 = 9.86960440$ . . ., whereas HRZCK gives only one: 9.78975. Deviation from this ideal problem, however, shows these results to be overly optimistic. Running uniform meshes for other

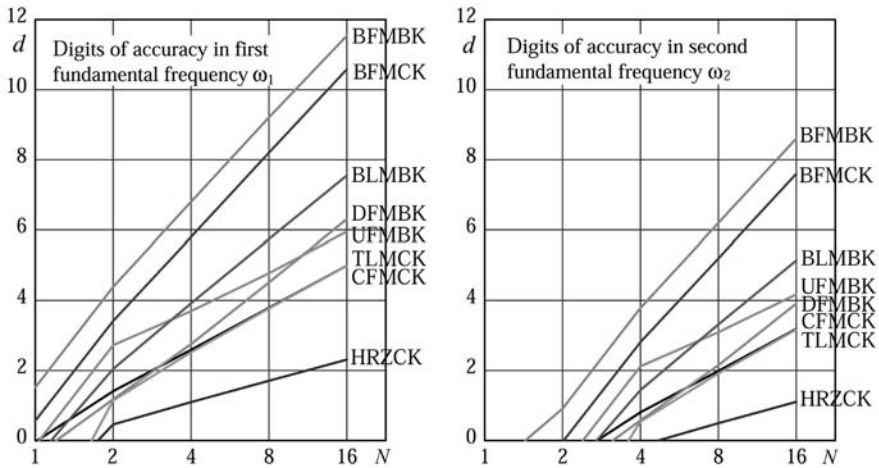

Figure 7.
Convergence of first two natural frequencies of SS uniform beam for the eight models of Table I, using a regular mesh of N elements

end conditions deliver lower accuracies and asymptotic rates, with BFMCK and BFMBK still winning but not by much. And mesh distortion is the great equalizer, as shown next.

Distortion sensitivity

To get a quick idea of the sensitivity of mass-stiffness combinations to mesh distortion, the SS beam with 16 elements is chosen. Every other interior node is displaced by $\ell\delta$ so elements have alternate lengths $\ell(1 \pm \delta)$. The loss of accuracy Δd in decimal places of the first two lowest frequencies is recorded as δ is increased from 0 to 0.50. Plots of Δd versus δ are shown in Figure 8. A steep $\Delta d(\delta)$ flags a combination with high distortion sensitivity. By far the most sensitive is BFMBK which loses close to six digits in ω_1 and five in ω_2 for $\delta \approx 0.5$. This is followed by BLMBK, which loses two to three digits, and then DFMBK, BFMCK and UFMBK, which lose one to two. Combinations TLMCK, CFMCK and HRZCK lose less than one digit, and can be viewed as fairly insensitive to distortion. Note that these last three combinations pertain to existing elements. These ratings are summarized in the last column of Table I. Rather than relying on numerical experiments it would be useful to have an explicit analytical expression of this kind of mesh sensitivity in terms of the parameters. This would simplify the design of a mass-stiffness combination attempting to meet both objectives A and S. Fourier analysis can be used for this task by examining plane wave propagation over an infinite periodic but irregular lattice. This is more laborious than regular lattice analysis because it involves a frequency equation of higher order, and remains to be done in the future.

Geometric stiffness analysis

Combinations of the geometric and material stiffness templates can be studied by similar Fourier techniques. These are simpler in that time does not enter the

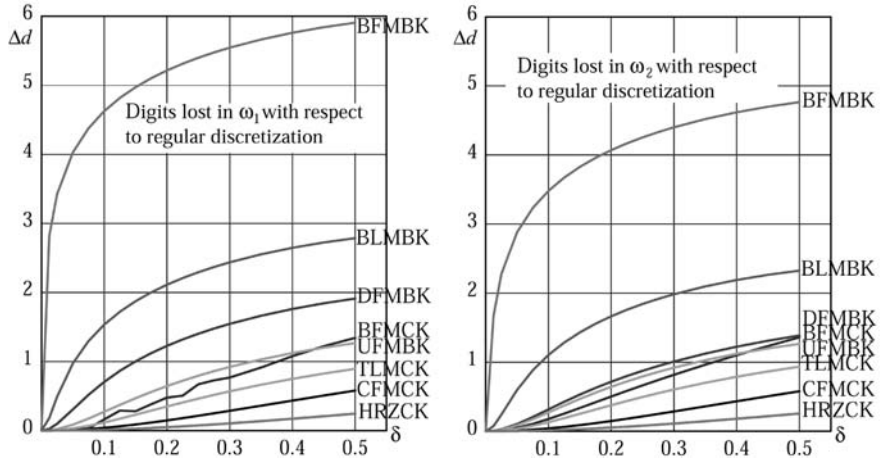

Figure 8.
Loss of accuracy in SS beam vibration analysis due to use of irregular mesh

analysis. The main objective is accurate prediction of buckling loads. The results will be reported in a more extensive paper.

Concluding remarks

Template forms of finite element matrices offer the opportunity of customizing FEM discretizations to achieve good performance for specific objectives. In the case of a general-purpose FEM program, which typically caters for a wide range of objectives, it is recommended that elements be programmed from the start using free parameters. These parameters can then be supplied through the argument list. An interesting extension not considered here is the Timoshenko beam model. Using templates this can be done by adjusting some of the free parameters to account for the shear properties. For instance, the material stiffness may be corrected by taking β as function of $GA_s/(12EI)$, in which GA_s is the cross-sectional shear rigidity, as described in Felippa (1994). In general only parameters associated with the L_4 cubic mode need to be adjusted. This is a simple and effective method to account for transverse shear. Rotational inertia can be similarly included in the mass matrix through the covariance matrix $\tilde{\mathbf{R}}$. In passing to 2D and 3D finite element models the following complications arise:

- The number of free parameters can be much higher. Incorporation of observer invariance and distortion sensitivity constraints from the start, as done for the plate bending triangle by Felippa (2000) using energy methods, is recommended because this formulation sequence reduces the dimension of the parameter space.
- The stiffness matrix of high performance elements is constructed through assumed stresses or strains, and a displacement field is generally available only on the boundaries.

So far only three-node flat triangle geometries for plane stress and bending have been studied in some detail at the material stiffness level. This is roughly the practical limit of symbolic manipulations with present hardware and CAS software. As desktop computers gain further processing power and storage address space, the approach should gradually become feasible for quadrilaterals and tetrahedral solid elements.

References

Abramowitz, M. and Stegun, L.A. (Eds) (1964), *Handbook of Mathematical Functions with Formulas, Graphs and Mathematical Tables*, Applied Mathematics Series 55, National Bureau of Standards, US Department of Commerce, Washington, DC.

Argyris, J.H., Kelsey, S. and Kamel, H. (1964), "Matrix methods of structural analysis – a precis of recent developments", in de Veubeke, B.M.F. (Ed.), *AGARDograph 72: Matrix Methods of Structural Analysis*, Pergamon Press, Oxford, pp. 1-164.

Belytschko, T. and Mullen, R. (1978), "On dispersive properties of finite element solutions", in Miklowitz, J. and Achenbach, J.D. (Eds), *Modern Problems in Elastic Wave Propagation*, Wiley, New York, NY, pp. 67-82.

Bergan, P.G. and Felippa, C.A. (1985), "A triangular membrane element with rotational degrees of freedom", *CMAME*, Vol. 50, pp. 25-69.

Bergan, P.G. and Hanssen, L. (1975), "A new approach for deriving 'good' finite elements", in Whiteman, J.R. (Ed.), *The Mathematics of Finite Elements and Applications – Volume II*, Academic Press, London, pp. 483-97.

Bergan, P.G. and Nygård, M.K. (1984), "Finite elements with increased freedom in choosing shape functions", *IJNME*, Vol. 20, pp. 643-64.

Brillouin, L. (1946), *Wave Propagation in Periodic Structures*, Dover, New York, NY.

Cook, R.D., Malkus, D.S. and Plesha, M.E. (1989), *Concepts and Applications of the Finite Element Analysis*, 3rd ed., Wiley, New York, NY.

Felippa, C.A. (1994), "A survey of parametrized variational principles and applications to computational mechanics", *CMAME*, Vol. 113, pp. 109-39.

Felippa, C.A. (1999), "Recent developments in basic finite element technologies", in Cheng, F.Y. and Gu, Y. (Eds), *Computational Mechanics in Structural Engineering – Recent Developments*, Elsevier, Amsterdam, pp. 141-56.

Felippa, C.A. (2000), "Recent advances in finite element templates", in Topping, B.J. (Ed.), *Proceedings of the CST 2000 and ECT 2000 Conferences*, Leuven, Belgium, September, Saxe-Coburn Publications, Edinburgh.

Felippa, C.A. and Militello, C. (1999), "Construction of optimal three-node plate bending elements by templates", *CM*, Vol. 24 No. 1, pp. 1-13.

Felippa, C.A., Haugen, B. and Militello, C. (1995), "From the individual element test to finite element templates: evolution of the patch test", *IJNME*, Vol. 38, pp. 199-222.

Graff, K.F. (1991), *Wave Motion in Elastic Solids*, Dover, New York, NY.

Hinton, E., Rock, T. and Zienkiewicz, O.C. (1976), "A note on mass lumping and related processes in the finite element method", *Earthquake Engrg Struct. Dynamics*, Vol. 4, pp. 245-9.

Malkus, D.S. and Plesha, M.E. (1986), "Zero and negative masses in finite element vibration and transient analysis", *CMAME*, Vol. 59, pp. 281-306.

Malkus, D.S., Plesha, M.E. and Liu, M.R. (1988), "Reversed stability conditions in transient finite element analysis", *CMAME*, Vol. 68, pp. 97-114.

Martin, H.C. (1966), "On the derivation of stiffness matrices for the analysis of large deflection and stability problems", in Przemieniecki, J.S. *et al.* (Eds), *Proceedings of the 1st Conference on Matrix Methods in Structural Mechanics*, AFFDL-TR-66-80, Air Force Institute of Technology, pp. 697-716.

Park, K.C. and Flaggs, D.L. (1984a), "An operational procedure for the symbolic analysis of the finite element method", *CMAME*, Vol. 46, pp. 65-81.

Park, K.C. and Flaggs, D.L. (1984b), "A Fourier analysis of spurious modes and element locking in the finite element method", *CMAME*, Vol. 42, pp. 37-46.